Aerosol Science and Technology

ISSN: 0278-6826 (Print) 1521-7388 (Online) Journal homepage: informahealthcare.com/journals/uast20

Investigation of Absorption and Scattering Properties of Soot Aggregates of Different Fractal Dimension at 532 nm Using RDG and GMM

Fengshan Liu, Cecillia Wong, David R. Snelling & Gregory J. Smallwood

To cite this article: Fengshan Liu, Cecillia Wong, David R. Snelling & Gregory J. Smallwood (2013) Investigation of Absorption and Scattering Properties of Soot Aggregates of Different Fractal Dimension at 532 nm Using RDG and GMM, Aerosol Science and Technology, 47:12, 1393-1405, DOI: 10.1080/02786826.2013.847525

To link to this article: https://doi.org/10.1080/02786826.2013.847525

Aerosol Science and Technology, 47:1393–1405, 2013

ISSN: 0278-6826 print / 1521-7388 online
DOI: 10.1080/02786826.2013.847525

Investigation of Absorption and Scattering Properties of Soot Aggregates of Different Fractal Dimension at 532 nm Using RDG and GMM

Fengshan Liu,[1] Cecillia Wong,[2] David R. Snelling,[1] and Gregory J. Smallwood[1]
[1]*Black Carbon Metrology, Measurement Science and Standards, National Research Council, Ottawa, Ontario, Canada*
[2]*Department of Chemical Engineering, Massachusetts Institute of Technology, Cambridge, Massachusetts, USA*

Radiative properties of numerically generated fractal soot aggregates of different fractal dimensions were studied using the numerically accurate generalized Mie-solution method (GMM) and the Rayleigh-Debye-Gans (RDG) approximate theory. Fractal aggregates of identical prefactor but different fractal dimensions, namely, 1.4, 1.78, and 2.1, were generated numerically using a tunable algorithm of cluster–cluster aggregation for aggregates containing up to 800 primary particles. Radiative properties of these aggregates were calculated at a wavelength of 532 nm assuming a soot refractive index of 1.6 + 0.6*i*. Four commonly used structure factors in the RDG approximation were used to investigate the effect of structure factor on the differential and total scattering cross-sections and the asymmetry factor. The differential and total scattering properties calculated using the RDG approximation become increasingly sensitive to the structure factor with increasing the fractal dimension. Primary particle interactions are the fundamental mechanism for the aggregate absorption enhancement for small aggregates and the shielding effect for larger aggregates. The extent of these two competing factors is dependent on the fractal dimension and aggregate size. RDG reasonably predicts the effect of fractal dimension on the scattering properties, but fails to account for the effect of aggregation or fractal morphology on the absorption property of fractal soot aggregates, though the error is in general less than 15%.

[Supplementary materials are available for this article. Go to the publisher's online edition of *Aerosol Science and Technology* to view the free supplementary files.]

Received 1 June 2013; accepted 9 September 2013.
The authors thank the financial support for this work from the PERD AFTER Program, Project C23.006, and AFTER11.
Address correspondence to Fengshan Liu, Black Carbon Metrology, Measurement Science and Standards, National Research Council, Building M-9, 1200 Montreal Road, Ottawa, ON K1A 0R6, Canada. E-mail: Fengshan.liu@nrc-cnrc.gc.ca

INTRODUCTION

Soot particles emitted from various combustion devices and fires are not only detrimental to human health (Brown et al. 2001; Oberdörster et al. 2004), but also form a climatically important class of tropospheric aerosols. Once emitted into the atmosphere soot is often called black carbon (BC) particles. It has been suggested that BC particles play important roles in affecting the environment and climate by directly altering the radiative properties of the atmosphere, visibility impairment, and cloud formation (Jacobson 2001; Zhang et al. 2008).

To adequately assess the importance of absorption of solar radiation by BC particles to the positive radiative forcing in the top of the atmosphere, it is essential to gain quantitative knowledge of their radiative properties. Unfortunately, the radiative properties of BC particles are still poorly quantified for the following reasons. First, BC particles are fractal aggregates formed by nearly identical spherical primary particles that have a complex and irregular fractal structure whose radiative properties in general cannot be predicted using the Mie theory developed for spherical particles. Second, the refractive index of BC particles is somewhat uncertain, possibly due to the different combustion conditions under which soot particles are formed. Third, the fairly open structure of soot particles emitted from various combustion devices tends to collapse into more compact clusters as they age in the atmosphere (Johnson et al. 1991; Reid and Hobbs 1998). Such a change in the soot morphology suggests that its radiative properties could also vary. Fourth, BC particles are often coated with various organic compounds as they age in the atmosphere. The coating also alters the absorption and scattering properties of BC particles, depending on the coating material and thickness (Lack and Cappa 2010) and the morphology of BC particles. It has also been known that coating causes BC particles to collapse into a compact structure (Mikhailov et al. 2001; Cross et al. 2010), which, in turn, alters their radiative properties. Although these factors make it difficult to accurately predict the radiative properties of BC particles, it is useful and important to understand how each factor affects the radiative properties of BC particles.

BC particles are formed by the aggregation of small, nearly identical and spherical primary particles into complex geometries that can be described by the following statistical scaling law (Forrest and Witten 1979):

$$N_p = k_f \left(\frac{R_g}{a}\right)^{D_f}, \quad [1]$$

where a is the radius of monomers (also called primary particles), N_p is the aggregate size (the number of primary particles contained in the considered aggregate), k_f and D_f are the fractal prefactor and fractal dimension, respectively, and R_g is the radius of gyration.

It is generally believed that fractal dimension is an important parameter in the description of fractal aggregates, such as combustion-generated soot particles, and is also a good indicator of the particle aggregation mechanism and aging processes (Adachi et al. 2007). Soot particles resulting from combustion or numerically simulated diffusion limited cluster aggregation (DLCA) exhibit fairly open structure with a fractal dimension in the range of 1.4–1.9 (Brasil et al. 2000). To date most studies on the radiative properties of fractal soot particles have focused on the evaluation of the accuracy and the range of the validity of the RDG approximation, (Farias et al. 1995; Farias et al. 1996; Van Hulle et al. 2002; Liu and Snelling 2008). A few studies have investigated the effect of the fractal parameters on the radiative properties of soot particles using more accurate numerical methods than the RDG approximation. Farias et al. (1996) evaluated the accuracy of the RDG theory for a wide range of primary particle size parameter ($x_p = 0.01$–1.0), refractive index ($|m$–$1| = 0.1$–2.0), and fractal dimension ($D_f =$ 1.0–3.0) by using the numerical results from the integral equation formulation for scattering (IEFS) as the reference solution. However, they only considered a fairly narrow range of aggregate size (represented by the number of primary particles) of $N_p = 16$–256 and the orientation averaged properties were achieved over only 16 orientations. Singham and Bohren (1993) investigated the scattering properties of two types of fractal aggregates using the coupled dipole method. The two types of fractal aggregates studied by Singham and Bohren were formed through the diffusion-limited aggregation (DLA), which leads to a quite compact structure with a fractal dimension about 2.5, and the diffusion-limited cluster aggregation (DLCA), which produces a less compact structure with a fractal dimension about 1.8. They found that the fractal dimension can have a large influence on some of the scattering matrix elements.

Liu et al. (2008) investigated the effect of fractal dimension on the radiative properties of soot fractal aggregates using the superposition T-matrix method for a wide range of fractal dimension from 1.25 to 3, two assumed refractive indices of $1.75 + 0.5i$ and $2 + i$, four aggregate sizes of $N_p = 200$, 400, 600, 800, and two primary particle diameters of 30 nm and 50 nm at a wavelength of 870 nm. Their results showed that the absorption cross-section of the aggregates formed by 30 nm primary particles tends to be relatively constant when $D_f < 2$ but increases rapidly with D_f when $D_f > 2$. They only presented numerical results of the absorption cross-section, total scattering cross-section, the single-scattering albedo, and the asymmetry parameter under the conditions of their investigation.

The effect of prefactor on the absorption and scattering properties of fractal soot aggregates was studied by Liu et al. (2009) using the generalized Mie-solution method (GMM) developed by Xu (1995, 1997) and the RDG theory for fractal soot aggregates having identical fractal dimension of $D_f = 1.78$ but two different prefactors of $k_f = 1.3$ and 2.3. They generated fractal aggregates of prescribed fractal parameters using a tunable cluster–cluster algorithm described by Liu and Snelling (2008), which was based on the algorithms developed by Filippov et al. (2000). The numerical calculations of Liu et al. (2009) were carried out at a relatively large primary particle size parameter of $x_p = 0.354$ and a typical soot refractive index in the visible range of $m = 1.6 + 0.6i$. Their results showed that for $N_p \geq 20$ the normalized absorption cross-section decreases with increasing the prefactor due to the stronger shielding effect as the aggregate becomes more compact. However, the normalized total scattering cross-section increases with increasing the prefactor as the scattered light by primary particles is more likely to be in-phase for a more compact aggregate.

Although several studies discussed above have investigated the effects of fractal dimension and prefactor on the radiative properties of soot aggregates, they either employed inadequate aggregate size or inadequate orientation averaging or only reported total scattering and absorption cross-sections. The present study conducted a numerical study to further investigate the effect of fractal dimension on the scattering and absorption properties of fractal soot aggregates in the visible using two well-established methods. One is the popular but less accurate RDG approximation and the other is the numerically exact GMM. Although the main objective of this study is to investigate the effect of fractal dimension on the radiative properties of fractal soot aggregates, the accuracy of the RDG approximation is also evaluated through a direct comparison between the RDG and GMM results with attention paid to the importance of the structure factor to the RDG results. The importance of multiple scattering on the radiative properties of fractal soot aggregates was also assessed using GMM.

THEORY

Numerical Generation of Fractal Aggregates

To conduct GMM calculations, it is necessary to provide the positions of constituent primary particles in a given aggregate. In this study, the positions of all the primary particles making up an aggregate of a given size are obtained through numerical generation of fractal aggregates. Different numerical methods have been developed to generate fractal aggregates formed by identical primary particles. These methods can be classified into two types: "mimicking" methods and tunable algorithms. The "mimicking" methods generate progressively larger aggregates by imposing a certain physical mechanism for their growth. In such methods the fractal parameters of the generated aggregates are not prescribed. Mimicking methods can be further divided into particle–cluster aggregation (PCA) and cluster–cluster aggregation (CCA) algorithms (Jullien and Botet 1987). PCA and CCA are also known as diffusion-limited aggregation (DLA) and diffusion limited cluster aggregation (DLCA), respectively (Singham and Bohren 1993). PCA generates aggregates with a fractal dimension of 2.5, while CCA generates aggregates with a fractal dimension of about 1.78 (Jullien and Botet 1987). The latter is in good agreement with the fractal dimension of combustion-generated soot. The pioneering fractal aggregate generation algorithms of the mimicking type have been reviewed by Jullien and Botet (1987). Unlike mimicking methods, tunable algorithms generate fractal aggregates of prescribed fractal dimension and prefactor by ensuring that during the growth of the aggregates the fractal scaling law given in Equation (1) is strictly satisfied. The tunable algorithms are developed to generate fractal aggregates of desired properties, regardless of the underlying physical mechanism. Typical tunable algorithms for fractal aggregate generation were described by Filippov et al. (2000) and the references cited therein. There are two distinct differences between mimicking methods and tunable algorithms. First, the fractal parameters (D_f and k_f) are prescribed in tunable algorithm, but not in mimicking methods. When a mimicking method is used to generate fractal aggregates, the fractal parameters are unknown a priori and governed by the particular growth mechanism (Jullien and Botet). Second, each aggregate generated using a tunable algorithm satisfies the scaling law given in Equation (1) with the prescribed D_f and k_f. However, it is not clear if individual aggregates generated using a mimicking method satisfy the scaling law of Equation (1) and only global fractal parameters can be derived from the ensemble of the generated aggregates. Because our objective is to investigate the sole effect of fractal dimension, it is essential to ensure that all the aggregates considered have the same prefactor and satisfy Equation (1). For these reasons, tunable algorithms were used in this study to generate fractal aggregates of desired D_f and k_f.

The radius of gyration R_g of an aggregate in Equation (1) is defined as (Filippov et al. 2000)

$$R_\mathrm{g}^2 = \frac{1}{N_\mathrm{p}} \sum_{i=1}^{N_\mathrm{p}} (\mathbf{r}_i - \mathbf{r}^0)^2 + \frac{3}{5}a^2, \quad [2]$$

$$\mathbf{r}^0 = \frac{1}{N_\mathrm{p}} \sum_{i=1}^{N_\mathrm{p}} \mathrm{r}_i, \quad [3]$$

where vectors $\mathbf{r}_i$ and $\mathbf{r}^0$ define the position of the ith primary particle center and the center of the aggregate, respectively. Although it has been known that BC particles become more compact as they age in the atmosphere, which is due at least partially to the effect of coating (Mikhailov et al. 2001), there is currently a lack of detailed knowledge on how the fractal parameters vary as the structure of the particles changes. In a recent study, Ouf et al. (2010) studied the morphology evolution of flame-generated soot as a function of storage duration in ambient air in the laboratory and found that D_f remained almost unchanged, while k_f and the degree of primary particle overlap increased slightly between 33 and 337 days. Because storage of soot in the laboratory does not closely mimic the ageing process of soot in the atmosphere, the findings of Ouf et al. (2010) cannot be used as direct evidence on how soot morphology evolves with ageing in the atmosphere. In the absence of further information, it is assumed in this study that the increase in the aggregate compactness as BC particles age in the atmosphere gives rise to an increase only in the fractal dimension, i.e., the prefactor remains unchanged. It is also known that there is up to about 20% overlap (or sintering), e.g., Ouf et al. (2010), between neighboring primary particles in BC aggregates, such effect is neglected in this study and primary particles are assumed to be in point touch.

Following the study of Filippov et al. (2000), small soot aggregates were first generated using the tunable particle–cluster aggregation or the sequential algorithm (SA). In this algorithm, identical spherical particles are added one by one to an existing aggregate (cluster) starting from an initial aggregate containing three point-touch primary particles. The newly added primary particle to the existing aggregate of size (N_p − 1) obey the following two rules: (i) it is in point-touch (no overlapping and no gap) with one of the primary particles in the aggregate with the touching point is randomly determined, and (ii) the newly generated larger aggregate always satisfies the scaling law, Equation (1). Further details of SA can be found in Filippov et al. (2000) and Liu and Snelling (2008).

SA was used to generate progressively larger aggregates up to $N_\mathrm{p} = 31$. Many different small aggregates of different sizes or different configurations of the same size were first generated by SA. These small aggregates were then used as the building blocks in the cluster–cluster aggregation (CCA) algorithm described below to generate even larger aggregates. To the best of our knowledge, there is no general guideline as to what the aggregate sizes generated by SA should be used as the building blocks of CCA. Our choice of using SA to generate aggregates up to $N_\mathrm{p} = 31$ is somewhat arbitrary and is based on considerations of efficiency and preserving the expected fractal aggregate property (see the online supplementary information). In this study, we fixed the prefactor at $k_\mathrm{f} = 2.3$, the primary particle radius $a = 15$ nm ($d_\mathrm{p} = 30$ nm), and three fractal dimensions $D_\mathrm{f} = 1.4$, 1.78, and 2.1. It should be noted that there is quite a large uncertainty in the value of prefactor for soot aggregates, ranging from 1.05 to 3.5 in the literature (Köylü et al. 1995;

Brasil et al. 2000). Our choice of $k_f = 2.3$ is somewhat arbitrary, but it is an intermediate value over the range of values reported in the literature and very close to the value of 2.4 determined experimentally by Köylü et al. (1995). It is worth pointing out that Sorensen and co-workers have found $k_f = 1.23$ and 1.7 in flame-soot experiments (Cai et al. 1995; Sorensen and Feke 1996) and DLCA simulations (Sorensen and Roberts 1997), though most of other studies of flame soot arrived at larger values of k_f (larger than 2, see summary of experimental data in Brasil et al. (2000)). As observed by Brasil et al. (2000), numerically simulated fractal aggregates in general have a fairly low prefactor (less than 1.5), while image analysis of real soot in general yields a prefactor greater than 2. The potential effect of overlap between monomers on the prefactor has been investigated by Oh and Sorensen (1997) and Brasil et al. (2000). Both groups found that there was an increase in the prefactor numerically derived from the known 3-D soot morphology. However, Oh and Sorensen (1997) further showed that there was also an increase in the numerically derived fractal dimension. Oh and Sorensen went further to show that if simulated 2-D images of soot aggregates with overlapped primary particles were analyzed by conventional experimental methods, ignoring any overlap, then fractal parameters very close to the nonoverlapped numeric values were obtained and concluded that they were unsuccessful in resolving the discrepancy between prefactors from real soot TEM images and those from simulations. Nevertheless, the present choice of $k_f = 2.3$ is higher than those of DLCA simulations of point-touch monomers.

The small aggregates generated using SA were then used to generate larger aggregates up to $N_p = 800$ using the cluster–cluster aggregation (CCA) algorithm described in detail in (Liu and Snelling 2008). At the beginning of CCA steps a larger aggregate is generated by merging two smaller aggregates generated using SA. Then even larger aggregates are generated by merging two newly generated aggregates using CCA. It should be emphasized that CCA, like SA, also preserve the prescribed D_f and k_f during each step of aggregate generation. Although there is no limitation to the size of aggregate that can be generated by SA, it is preferred not to use SA to generate large aggregates. It has been shown by Filippov et al. (2000) that the density autocorrelation function of aggregates generated using the particle–cluster method (SA) on a log–log scale displays a slope that is different from the expected value of (3-D_f). Consequently, systematic errors can occur if these aggregates are used to study the physical and scattering properties of fractal aggregates. Filippov et al. (2000) also showed that the density autocorrelation function for aggregates generated by the tunable CCA algorithm do exhibit a consistent slope as expected from the specified fractal dimension when the aggregates are large enough. Therefore, the CCA algorithm was used to generate large aggregates.

For a given set of morphological parameters (d_p, N_p, D_f, k_f), there are endless possibilities for the positions of primary particles that satisfy the scaling relationship given in Equation (1), but result in somewhat different scattering properties. To minimize the effect of a specific aggregate configuration/realization on the scattering properties of a randomly oriented ensemble of monodisperse fractal aggregates, ten different aggregate realizations of identical morphological parameters (d_p, N_p, D_f, k_f) were generated based on a recent study (Liu and Smallwood 2010a), where it was shown that averaging over ten realizations is adequate to achieve realization independent radiative properties of soot fractal aggregates.

The advantage of the tunable algorithm for aggregate generation is that all the aggregates of different sizes have identical fractal parameters as specified. Therefore, the aggregates generated from tunable algorithms are suitable for investigating the effect of an individual parameter, such as the fractal dimension or the prefactor, on various physical and scattering properties of fractal aggregates. As pointed out by Liu et al. (2008), however, for each value of the prefactor (or the fractal dimension) there is only a relatively narrow range of fractal dimension (or the prefactor) that allows the aggregates of specified fractal parameters and of point-touch primary particles to be generated. For the chosen value of $k_f = 2.3$, higher values of D_f greater than 2.1 do not allow generation of fractal aggregates that fulfill all the requirements. This is why the present investigation is limited to a maximum D_f value of 2.1. Such a restriction in the selection of D_f and k_f in tunable algorithms for fractal aggregation generation is likely a manifestation of the possible relationship between D_f and k_f, as suggested in several studies (Sorensen and Roberts 1997; Gmachowski 2002; Lapuerta et al. 2006; Heinson et al. 2012).

Rayleigh-Debye-Gans Fractal Aggregate Theory

Application of the RDG theory to fractal soot aggregates requires the following conditions to be fulfilled (Bohren and Huffman 1983; Kerker 1969): (i) $|m - 1| \ll 1$ and $2x_p |m - 1| \ll 1$ with $m = n + ki$ being the refractive index of the particle material and $x_p = \pi d_p/\lambda$ the size parameter of primary particle, (ii) the effects of multiple scattering induced by other particles in the aggregate and self-interaction of the primary particle itself are negligible. These assumptions imply that each primary particle is in the Rayleigh regime and acts as a dipole source for scattered radiation. As observed by Köylü and Faeth (1993, 1994), the first assumption is not satisfactorily met by soot due to its relatively large refractive index. Even so, previous studies showed that RDG in general produces reasonably accurate results for the scattering properties of soot (Dobbins and Megaridis 1991; Farias et al. 1996). Multiple scattering within a fractal aggregate was found small in several studies (Berry and Percival 1986; Singham and Bohren 1993; Mulholland et al. 1994; Farias et al. 1996).

The radiative cross-sections of primary particles can be written as (Köylü and Faeth 1994),

$$C^p_{\text{abs}} = 4\pi x_p^3 E(m)/k^2,\ C^p_{\text{sca}} = 8\pi x_p^6 F(m)/(3k^2),$$
$$C^p_{\text{vv}} = x_p^6 F(m)/k^2, \quad [4]$$

where $k = 2\pi/\lambda$ is the wave number, $E(m)$ and $F(m)$ are functions of the complex refractive index of soot m with $E(m) = Im((m^2 - 1)/(m^2 + 2))$ and $F(m) = |(m^2 - 1)/(m^2 + 2)|^2$. Subscripts abs, sca, and vv represent absorption, total scattering, and vertical (for incident radiation) and vertical (for scattered radiation) polarized differential scattering, respectively. Superscript p indicates properties of primary particles. The scattering cross-sections of an aggregate for polarized light are given as (Köylü and Faeth 1994; Sorensen 2001),

$$C_{\mathrm{vv}}^{\mathrm{agg}}(\theta) = C_{\mathrm{hh}}^{\mathrm{agg}}(\theta)/\cos^2\theta = N_{\mathrm{p}}^2 C_{\mathrm{vv}}^{p} S(qR_g), \qquad [5]$$

where superscript agg represents quantities of aggregate, θ is the scattering angle, $q = 2k\sin(\theta/2)$ is the modulus of scattering vector, and $S(qR_{\mathrm{g}})$ is the aggregate structure factor. Several different expressions for the structure factor have been reviewed by Sorensen (2001). In this study, four structure factor expressions were considered to investigate how the structure factor affects the scattering properties of soot fractal aggregates. The four structure factors investigated are those used by Dobbins and Megaridis (1991), Köylü and Faeth (1994), Sorensen et al. (1992), and Yang and Köylü (2005). These structure factors are summarized in Table 1. The structure factor proposed by Sorensen et al. (1992) has no connection to the other three and was derived from the Fourier transformation of the density autocorrelation function assuming a Gaussian cut-off function. The structure factor used by Dobbins and Megaridis (1991) was based on using the Guinier formula at small qR_{g} and the expected power law behavior at large qR_{g} with a condition of continuity in the function and its slope where they meet. The boundary between the small qR_{g} regime, or the so-called Guinier regime, and large qR_{g} regime, or the power-law regime, was taken as

$$(qR_g)^2 = 3D_f/2. \qquad [6]$$

The structure factor used by Köylü and Faeth (1994) is identical to that of Dobbins and Megaridis (1991) except that, in the large qR_{g} regime, the factor $(3D_{\mathrm{f}}/2e)^{\mathrm{Df}/2}$, was neglected. This factor is actually important to ensure the continuity of the structure factor at the boundary defined in Equation (6). Although for $D_{\mathrm{f}} = 1.8$ the factor $(3D_{\mathrm{f}}/2e)^{\mathrm{Df}/2}$ is very close to 1.0 (0.99), its value departs from unity for smaller and larger D_{f}. For example, the constant $(3D_{\mathrm{f}}/2e)^{\mathrm{Df}/2}$ is 0.84 for $D_{\mathrm{f}} = 1.4$ and 1.17 for $D_{\mathrm{f}} = 2.1$. Therefore, neglect of this factor can introduce larger errors for D_{f} different from about 1.8. The structure factor of Yang and Köylü (2005) is a unified expression of Köylü and Faeth (1994) connecting the small and large qR_{g} regimes with a single expression. Therefore, it is expected that the Yang and Köylü (2005) structure factor has a broadened transition between the Guinier and the power-law regime.

Once a structure factor is selected, the differential scattering cross-section can be obtained directly from Equation (5). The total scattering cross-section for unpolarized incident light can then be calculated as

$$C_{\mathrm{sca}}^{\mathrm{agg}} = N_{\mathrm{p}}^2 C_{\mathrm{vv}}^{p} 2\pi \int_0^{\pi} S(qR_g)\frac{1}{2}(1+\cos^2\theta)\sin\theta d\theta. \qquad [7]$$

By using the linearized approximation for the exponential function in the entire Guinier regime for small value of qR_{g} (up to the boundary) of the Köylü and Faeth (1994) structure factor given in Table 1, i.e., $\exp[-(qR_g)^2/3] \approx 1 - (qR_g)^2/3$, Köylü and Faeth (1994) obtained an analytical expression for the total scattering cross-section. Except for the Köylü and Faeth total scattering cross-section, which was calculated using their analytical expression, the total scattering cross-sections for unpolarized incident light associated with the other three structure factors are calculated numerically using Equation (7).

In RDG approximation, the interactions among primary particles are completely neglected as far as absorption is concerned. Therefore, the aggregate absorption cross-section is simply the summation of all the primary particle cross-sections, i.e.,

$$C_{\mathrm{abs}}^{\mathrm{agg}} = N_{\mathrm{p}} C_{\mathrm{abs}}^{p}. \qquad [8]$$

Another important parameter in assessing the contribution of BC particles to radiative forcing in atmosphere is the asymmetry

TABLE 1

Four different expressions for the structure factor considered in this study

Researchers	$S(qR_{\mathrm{g}})$	
Dobbins and Megaridis (1991)[1]	$S(qR_g) = \exp[-(qR_g)^2/3]$	for small qR_{g}
	$= (3D_f/2e)^{D_f/2}(qR_g)^{-D_f}$	for large qR_{g}
Köylü and Faeth (1994)	$S(qR_g) = \exp[-(qR_g)^2/3]$	for small qR_{g}
	$= (qR_g)^{-D_f}$	for large qR_{g}
Sorensen et al. (1992)[2]	$S(qR_g) = \exp[-(qR_g)^2/D_f] \times {}_1\mathrm{F}_1[\frac{3-D_f}{2}, \frac{3}{2}, \frac{(qR_g)^2}{D_f}]$	
Yang and Köylü (2005)	$S(qR_g) = [1 + 8(qR_g)^2/(3D_f) + (qR_g)^8]^{-D_f/8}$	

[1] e is the base of natural logarithm.

[2] ${}_1\mathrm{F}_1$ is the Kummer or confluent hypergeometric function.

factor. This quantity is related to the scattering phase function and is defined as (Bohren and Huffman 1983)

$$g = \overline{\cos\theta} = \int_{4\pi} p(\theta)\cos\theta d\Omega, \quad [9]$$

where $p(\theta)$ is the scattering phase function and Ω is the solid angle. The scattering phase function is defined as (Bohren and Huffman 1983)

$$p(\theta) = \frac{1}{C_{\mathrm{sca}}^{\mathrm{agg}}} \frac{C_{\mathrm{vv}}^{\mathrm{agg}} + C_{\mathrm{hh}}^{\mathrm{agg}}}{2}. \quad [10]$$

The asymmetry factor is between -1 and 1 and characterizes how the scattered radiation is distributed. For example, $g > 0$, $=0$, and < 0 correspond to forward scattering, isotropic scattering, and backward scattering, respectively.

Generalized Mie-Solution Method

Two methods have been developed in the literature to obtain numerically exact radiative properties of an object formed by nonoverlapping spherical monomers. One is the cluster T-matrix method (CTM) (Mishchenko 1991; Khlebtsov 1992). The other one is the generalized Mie-solution method (GMM). GMM was developed by Xu (1995, 1997) based on the framework of the Mie theory for a single sphere and the addition theorems for spherical vector wave functions. It provides a rigorous and complete solution to nonoverlapping multisphere light scattering problems and can be readily applied to fractal soot aggregates (Van-Hulle et al. 2002; Liu and Snelling 2008). Execution of this numerically exact method requires the positions, diameter, and refractive index of each constituent sphere (primary particle). Although CTM has become the most popular method to study the radiative properties of various scatterers (Mishchenko et al. 2008), GMM has also been demonstrated to be a powerful tool to study radiative properties of various particles (Xu 1995, 1997; Van-Hulle et al. 2002; Liu and Snelling 2008). In fact, CTM and GMM share a very similar theoretical framework, though differences exist (Xu and Khlebtsov 2003). GMM offers some advantages over CTM according to Xu and Khlebtsov (2003). GMM rigorously accounts for the multiple scattering within the aggregate. However, GMM is computationally very demanding and memory intensive for large aggregates containing several hundreds of primary particles. GMM is used in this study for the reason that it offers the capability of quantifying the effect of multiple scattering.

RESULTS AND DISCUSSION

All the calculations were conducted at an incident wavelength of $\lambda = 532$ nm. A typical value of the refractive index of soot in the visible, $m = 1.6 + 0.6i$, was assumed at the wavelength considered. Calculations were conducted up to $N_{\mathrm{p}} = 800$. The GMM results were first averaged over more than 29,000 orientations for $N_{\mathrm{p}} \leq 200$ and over more than 9000 orientations for larger aggregates. The orientation-averaged GMM results were then used for realization averaging. The GMM results reported in this study were obtained for 10 realizations for all the aggregate sizes computed between $N_{\mathrm{p}} = 10$ to 800, based on a previous study (Liu and Smallwood 2010a). Unless otherwise stated, all the GMM results presented below were obtained with the interactions among primary particles taken into account.

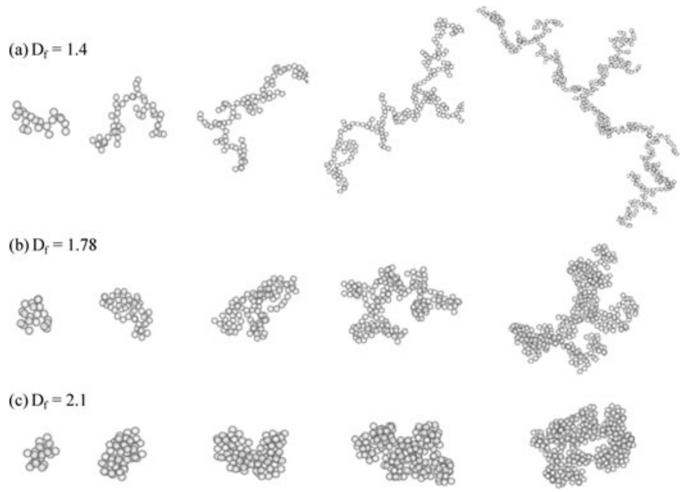

FIG. 1. Typical fractal aggregates generated using the tunable cluster–cluster aggregation algorithm, except the smallest aggregates shown for $N_{\mathrm{p}} = 20$. These aggregates are of size $N_{\mathrm{p}} = 20$, 50, 100, 200, and 400, respectively, for (a) $D_{\mathrm{f}} = 1.4$, (b) $D_{\mathrm{f}} = 1.78$, and (c) $D_{\mathrm{f}} = 2.1$. In all cases, $k_{\mathrm{f}} = 2.3$ and $d_{\mathrm{p}} = 30$ nm.

To illustrate how the structure of fractal aggregates varies with the fractal dimension while keeping the prefactor constant, Figure 1 displays the typical appearance of fractal aggregates for $D_{\mathrm{f}} = 1.4$, 1.78, and 2.1 while keeping the prefactor constant at $k_{\mathrm{f}} = 2.3$.

As shown in the online supplementary information, the numerical aggregates generated in this work using CCA do display the correct slope in the density autocorrelation function for sufficiently large aggregates. The autocorrelation function was calculated as the distance distribution function described by Hasmy et al. (1993) and Filippov et al. (2000).

Effect of D_f on RDG Vertical-Vertical Differential Scattering Cross-Section

Although differential scattering properties are not directly required in assessing the contribution of BC particles to the positive radiative forcing in atmosphere, they are highly desirable in the interpretation of elastic light scattering measurements for obtaining morphological information of soot particles in various applications (Sorensen 2001). The first part of this section is dedicated to the effect of different structure factors on the RDG results.

The nondimensional vv differential cross-sections (normalized by $N_{\mathrm{p}}^2 C_{\mathrm{vv}}^p$) predicted by RDG with the four structure factors summarized in Table 1 are compared in Figures 2 and 3 for $N_{\mathrm{p}} = 50$, and 200, respectively, plotted against a

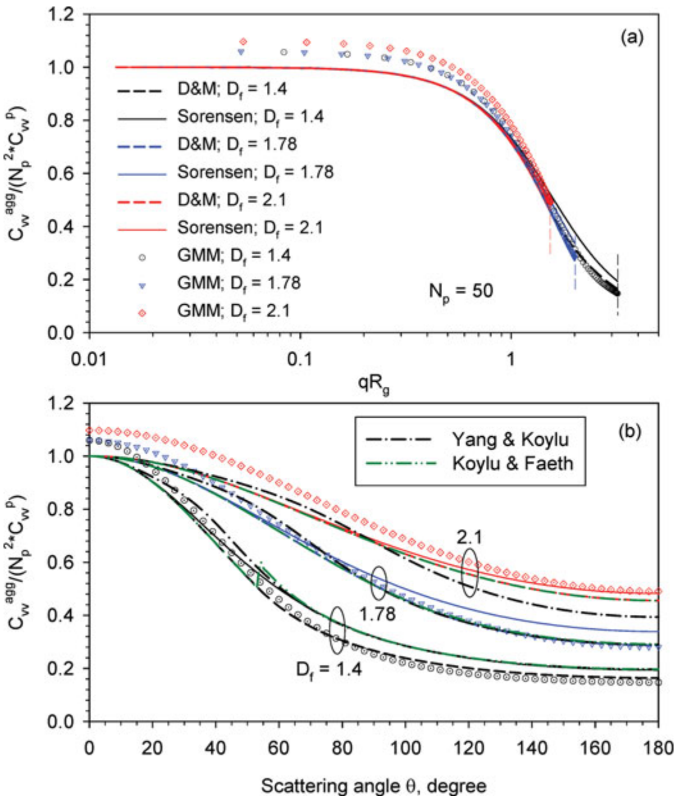

FIG. 2. Comparison of RDG nondimensional vertical–vertical differential scattering cross-sections with four different structure factors for monodisperse aggregates of $N_{\mathrm{p}} = 50$ and different fractal dimensions: (a) against qR_{g}, (b) against the scattering angle θ. In all cases, $\lambda = 532$ nm, $d_{\mathrm{p}} = 30$ nm, and $k_{\mathrm{f}} = 2.3$. The corresponding GMM results are also plotted. (Color figure available online.)

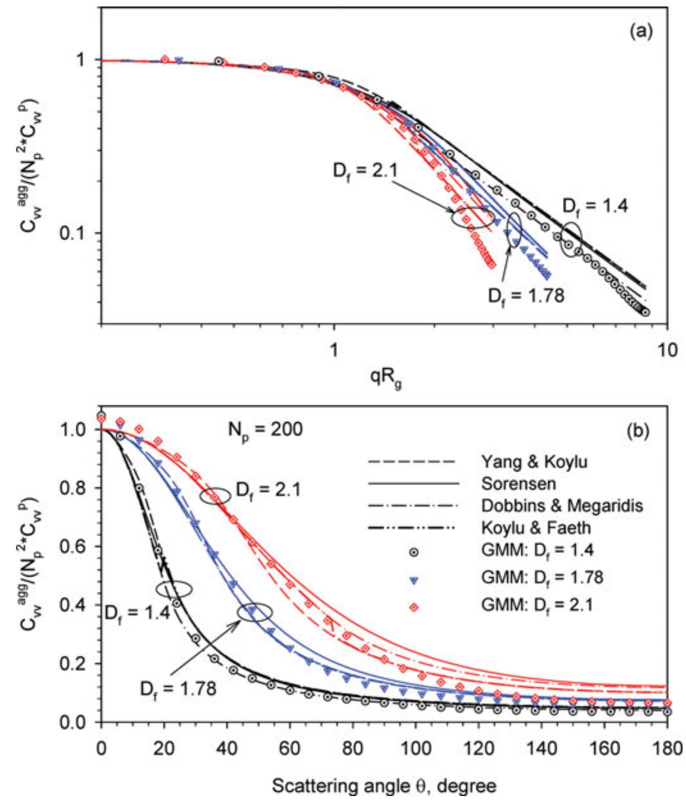

FIG. 3. Comparison of RDG nondimensional vertical–vertical differential scattering cross-sections with four different structure factors for monodisperse aggregates of $N_{\mathrm{p}} = 200$ and different fractal dimensions: (a) against qR_{g}, (b) against the scattering angle θ. In all cases, $\lambda = 532$ nm, $d_{\mathrm{p}} = 30$ nm, and $k_{\mathrm{f}} = 2.3$. The corresponding GMM results are also plotted. (Color figure available online.)

nondimensional variable qR_{g} and/or the scattering angle θ. As a result of such normalization, the vv differential cross-section is identical to the structure factor when plotted against qR_{g}. qR_{g} is an important nondimensional parameter as far as scattering by fractal aggregate is concerned (Sorensen 2001). Plotting the variation of vv scattering cross-section with the scattering angle is also very informative, since it shows at what angles the scattered light should be detected that are most important experimentally in retrieving the soot particle morphological parameters. The RDG vv scattering cross-sections of Yang and Köylü and Köylü and Gaeth are not plotted in Figure 2a for clarity. The effects of structure factor and the fractal dimension are evident.

The first observation from these figures is that these structure factors display rather large differences. These figures clearly show that the nondimensional vv scattering cross-sections decay slower with the scattering angle as the fractal dimension increases, Figures 2b and 3b. It is also evident from Figures 2b and 3b that vv scattering becomes not only much stronger, but also increasingly dominant in the forward direction as the aggregate size increases.

Results based on the structure factor of Köylü and Faeth (1994) display a discontinuity in the vv scattering cross-section at the boundary of small and large qR_{g} values, which is clearly shown in Figure 2b at a scattering angle of about 50° for $D_{\mathrm{f}} = 1.4$, where the vv scattering cross-section jumps from a smaller Guinier regime value to a larger power-law regime one. Such a discontinuity is caused by neglecting the factor $(3D_{\mathrm{f}}/2e)^{D\mathrm{f}/2}$ in the power-law regime expression. The discontinuity is invisible for $D_{\mathrm{f}} = 1.78$ occurring around $\theta = 112°$, because the missing factor in this case is very close to unity. There is no discontinuity for $D_{\mathrm{f}} = 2.1$ in Figure 2b, simply because the power-law regime is not reached for $N_{\mathrm{p}} = 50$ in this case. The discontinuity in the vv scattering cross-section for a larger aggregates of $N_{\mathrm{p}} = 200$, Figure 3b, can be clearly seen for $D_{\mathrm{f}} = 1.4$, and 2.1. As expected, results from the other three structure factors all vary smoothly with either qR_{g} or the scattering angle. Figure 3a also shows that for given morphology of monodisperse fractal aggregates (D_{f}, k_{f}, N_{p}, a), there exists a maximum qR_{g}, whose value is dependent on the wavelength and R_{g}. The more open the aggregate structure, the larger value the maximum qR_{g} can reach. The implication of this fact is that the power-law regime may not be reached when the light scattering measurements are conducted for a selected wavelength.

Although the RDG vv scattering cross-section based on the four structure factors display somewhat significant differences in the transition regime of intermediate qR_g values between the Guinier and power-law regimes, these results share two common features: (1) they are identical in the limit of small qR_g, i.e., in the forward directions of very small θ, and (2) they have the same slope of $-D_f$ on the log–log plot in the limit of large qR_g. In Figure 3a, where $N_p = 200$, for $D_f = 1.4$ the power-law regime is reached when qR_g is greater than about 1.5, where the result of Köylü & Faeth exhibits a sudden jump, in all the results. However, the power-law regime is not reached for the other two aggregates of larger fractal dimensions in the results of Sorensen structure factor.

In summary, the RDG results of vv scattering cross-section using the four different structure factors differ significantly from one another. The structure factor of Köylü and Faeth (1994) suffers a discontinuity at the boundary of the Guinier and power-law regimes when D_f deviates from 1.812 ($2e/3$) and, therefore, should not be used in the interpretation of light scattering measurements. The empirical fit of Yang and Köylü (2005) tends to overpredict the scattering at small angles and underpredict scattering at large angles when compared to the results of Sorensen (2001) or Dobbins and Megaridis (1991). Overall, the results of Sorensen are in closer agreement with those of Dobbins & Megaridis than those of Yang & Köylü for $D_f = 1.78$ and 2.1. For more open aggregates of $D_f = 1.4$, however, the opposite trend is observed, i.e., the vv scattering cross-sections based on the structure factor of Dobbins & Megaridis are lower. Only the structure factors of Sorenson (2001) and Dobbins and Megaridis (1991) are considered in the next section.

Comparison of RDG and GMM Results

The nondimensional vv differential scattering cross-sections of monodisperse ensembles of randomly oriented aggregates calculated from RDG and GMM are compared in Figures 2–4 for $N_p = 50$, 200, and 800, respectively. Again, the vv scattering cross-sections are plotted against both qR_g and the scattering angle θ for reasons mentioned earlier. The overall variations of the vv scattering cross-section with the aggregate size and the fractal dimension have been discussed earlier. The focus here is the difference between RDG and GMM results and the variation of the GMM results with the fractal dimension.

The vertical dotted lines in Figure 2a indicate the maximum qR_g values corresponding to the three fractal dimensions considered. The nondimensional vv scattering cross-sections from RDG are always exactly equal to unity in the forward direction ($\theta = 0°$). The nondimensional vv scattering cross-sections from GMM are generally greater than unity in the low $qR_\mathbf{g}$ (angle) limit. The degree by which the GMM results overshoot unity decreases with increasing aggregate size, and the nondimensional vv scattering cross-sections of $N_p = 800$ and $D_f = 2.1$ are actually lower than unity in the forward directions (Figure

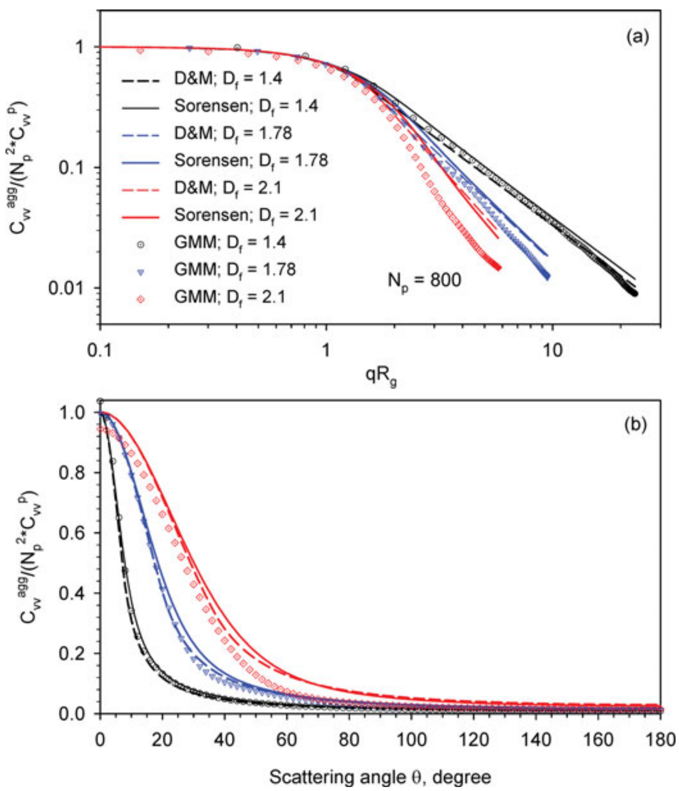

FIG. 4. Comparison of nondimensional vertical–vertical differential scattering cross-sections predicted by RDG and GMM for ensembles of monodisperse aggregate of $N_p = 800$ and different fractal dimensions: (a) against qR_g, (b) against the scattering angle θ. In all cases: $\lambda = 532$ nm, $d_p = 30$ nm, and $k_f = 2.3$. (Color figure available online.)

4b). It is noted that the degree of such overshoot is not only dependent on the aggregate size, but is also dependent on the fractal dimension. For fairly small aggregates of $N_p = 50$ (Figure 2b), the non-dimensional vv scattering cross-sections of the most compact aggregate of $D_f = 2.1$ exhibit the largest deviation from the RDG results than those of the less compact aggregates, especially in the forward directions. For larger aggregates of $N_p = 200$ (Figure 3b), the nondimensional GMM vv scattering cross-sections of the three aggregates of different D_f are almost identical in the forward directions and slightly higher than unity. For even larger aggregates of $N_p = 800$, the GMM vv scattering cross-section in the forward directions actually decreases with increasing fractal dimension (Figure 4b). The overall variations of the vv scattering cross-section with the aggregate size and the fractal dimension calculated from GMM are in qualitative agreement with those from RDG, i.e., scattering is enhanced with both the aggregate size N_p and the fractal dimension D_f, except for very large compact aggregates in the forward directions. The GMM results depart more significantly from the RDG values with increasing the fractal dimension at large qR_g values, where the GMM results are lower than those of RDG that lead to a slope less than $-D_f$, see Figures 3a and 4a. This trend has been observed in several previous studies (Liu and Snelling

2008; Yon et al. 2008; Liu et al. 2009). Liu et al. (2009) and Yon et al. (2008) explained the deviation of the GMM results from the RDG ones at large qR_g values in terms of the role of multiple scattering. Although this explanation is qualitatively plausible, results from additional GMM calculations without interactions among primary particles for fractal soot aggregates with $D_f = 1.78$ indicate that the multiple scattering effect is quite small and is not the primary cause for the discrepancy between the GMM and RDG results at large qR_g values in Figures 3 and 4. Further research is required to understand the reasons responsible for this discrepancy.

To explore the importance of the interactions among primary particles to the departure from unity in the GMM nondimensional vv scattering cross-section in the forward directions, additional GMM calculations without the primary particle interaction were performed for the compact aggregates of $D_f = 2.1$ and different sizes. Comparisons of these results (not shown) with those with primary particle interaction indicate that the departure of the nondimensional GMM vv scattering cross-sections from unity in the forward directions is indeed primarily attributed to the interactions among primary particles (the secondary factor affecting such departure is the non-Rayleigh scattering behavior of primary particles). Such interactions enhance scattering for all directions, especially in the forward directions, for relatively small aggregates, e.g., $N_p = 50$, but otherwise weaken scattering in all directions for large aggregates, e.g., $N_p = 800$. The enhancement of scattering due to primary particle interactions (interference effect) for relatively small aggregates, especially as the compactness of the aggregate increases (with increasing D_f), is also revealed in the enhancement of aggregate absorption cross-sections shown below.

Effect of Fractal Dimension on the Total Scattering Cross-Section

Variations of the nondimensional total scattering cross-sections (normalized by $N_p C_{sca}^p$) calculated using RDG and GMM with the aggregate size for aggregates of three different fractal dimensions are shown in Figure 5. The normalized total scattering cross-sections increase with the aggregate size as well as the fractal dimension. Although the structure factor of Köylü and Faeth (1994) consists of an error (missing a factor), its results are still included in Figure 5 to illustrate how the missing factor affects the total scattering cross-sections. It is noticed from Figure 5 that there is a dip in the results of Köylü and Faeth and the extent of the dip increases with increasing fractal dimension. The dip occurs at an aggregate size corresponding to $\beta = 3D_f/(8k^2R_g{}^2) = 1$, which is related to the boundary between the Guinier and power-law regimes given in Equation (6). The dip in the total scattering cross-section of Köylü and Faeth is attributed to the linearization of the exponential expression in the entire Guinier regime (up to the boundary) and has been previously observed by Kazakov and Frenklach (1998). For the relatively open aggregates of $D_f = 1.4$, Figure 5c, the RDG total scattering cross-sections from different structure factors are in close agreement with each other, except those from Dobbins and Megaridis at relatively large aggregates beyond about $N_p = 50$, where the total scattering cross-sections of Dobbins and Megaridis are lower than those from the other three structure factors. The discrepancies in the total scattering cross-section between the RDG results of different structure factors increase with the fractal dimension. For aggregates of $D_f = 1.78$, Figure 5b, and 2.1, Figure 5a, the total scattering cross-sections of Köylü and Faeth are the lowest among the RDG results, while results from the other three structure factors agree well with each other. Among the RDG results, the total scattering cross-sections from the structure factor of Sorensen are the highest under all three fractal dimensions. The overall agreement between the GMM and RDG results is fairly good with GMM results being slightly higher for small aggregates and slightly lower for large aggregates.

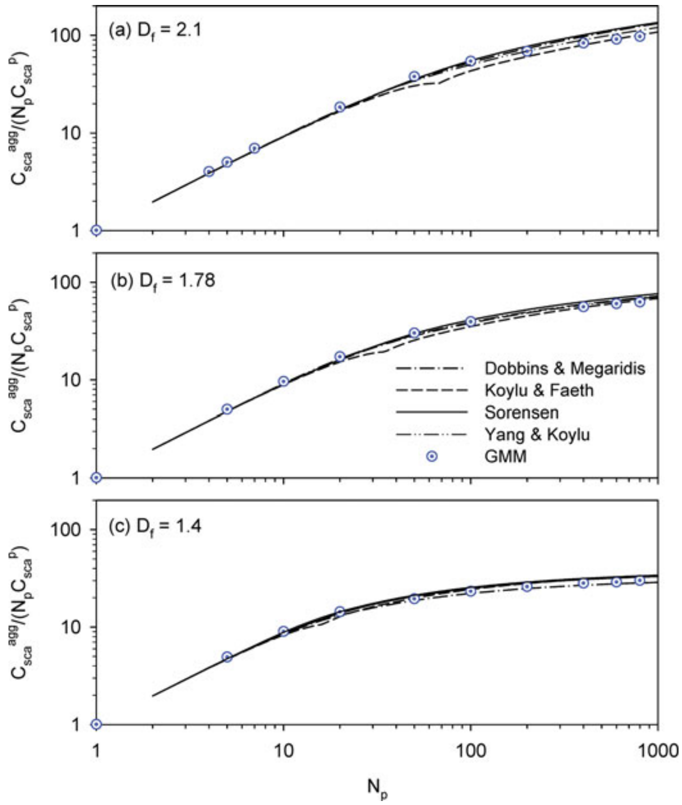

FIG. 5. Variation of the nondimensional total scattering cross-section with aggregate size for aggregates of different fractal dimensions: (a) $D_f = 2.1$, (b) $D_f = 1.78$, and (c) $D_f = 1.4$. (Color figure available online.)

Effect of Fractal Dimension on the Asymmetry Factor

Variations in the asymmetry factor from RDG with the structure factors of Sorensen and Dobbins & Megaridis with aggregate size are compared to those from GMM for aggregates of different fractal dimensions in Figure 6. Although there are differences between the two RDG results and between RDG and GMM results, both RDG and GMM predict a similar overall

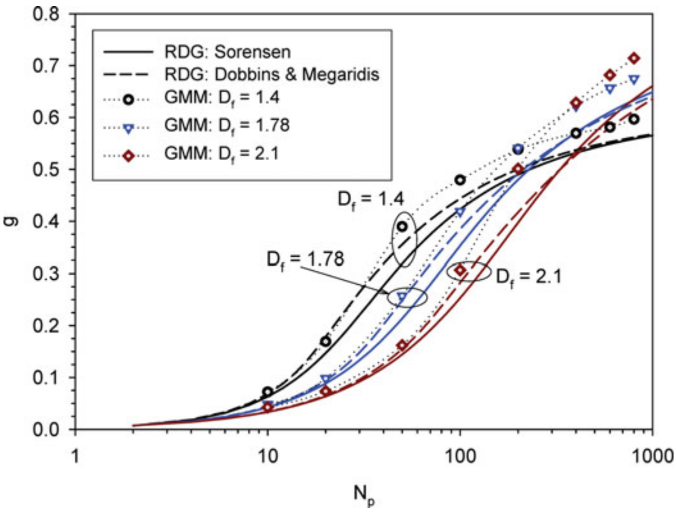

FIG. 6. Variation of the asymmetry factor with aggregate size for monodisperse aggregates of different fractal dimension. (Color figure available online.)

trend of variation of the asymmetry factor with aggregate size and fractal dimension. The asymmetry factor increases with the aggregate size, suggesting that the scattering pattern becomes increasingly dominant in the forward direction, which has been observed from the vv scattering cross-sections shown earlier in Figures 2–4. The two RDG results display relatively large differences from each other for a range of intermediate aggregate size and this range of aggregate size shifts towards larger aggregates as the fractal dimension increases. Variation of the asymmetry factor with the fractal dimension exhibits interesting features from both the RDG and GMM results: it first decreases for relatively small aggregates (less than about $N_p = 200$) as the fractal dimension increases and then increases more rapidly to reach higher values for large aggregates. The decrease in the asymmetry factor with increasing fractal dimension for relatively small aggregates may be explained by the increase in the compactness of the aggregates as D_f increases (becoming more sphere-like), since scattering by small spherical particles tends to be more isotopic (corresponding to lower asymmetry factors).

The asymmetry factors from RDG are in good agreement with those from GMM only for very small aggregates. In general, RDG underpredicts the asymmetry factor for intermediate and large aggregates under all three fractal dimensions considered.

The overall variation trend of the GMM asymmetry factor with the aggregate size N_p or the fractal dimension D_f is qualitatively similar to that obtained by Liu et al. (2008) though differences are observed. For example, for aggregates of size 200 Figure 6 shows that the asymmetry factor for $D_f = 1.4$ is almost the same as that for $D_f = 1.78$, but it becomes smaller at a higher fractal dimension of $D_f = 2.1$. The results of Liu et al. (2008) (for $m = 1.75 + 0.5i$) showed that the asymmetry factor for aggregates of size 200 peaks at about $D_f = 1.5$ and starts to decrease with increasing D_f. Differences also exist between our results shown in Figure 6 and those of Liu et al. (2008) for larger aggregates. For the largest aggregates of size 800 investigated, the asymmetry factor increases monotonically in the fractal dimension range of 1.4 to 2.1 shown in Figure 6. The results of Liu et al. (2008), however, showed that the asymmetry factor peaks at $D_f = 1.75$ and then starts to decrease slowly in the D_f range of 1.75 and 2.25 before dropping rapidly for even larger fractal dimensions. Based on the study of Liu et al. (2008), who showed similar results for $m = 1.75 + 0.5i$ and $m = 2 + i$, the discrepancies between our results shown in Figure 6 and those of Liu et al. (2008) are not caused by the difference in soot refractive index. A plausible explanation for the discrepancies lies in the difference in the wavelength. However, this conjecture remains to be confirmed.

Effect of Fractal Dimension on Absorption Cross-Section

Variation of the nondimensional aggregate absorption cross-sections (normalized by $N_p C^p_{abs}$) from RDG and GMM with aggregate size for aggregates of different fractal dimensions are compared in Figure 7. The nondimensional absorption cross-sections from RDG remain at unity regardless of aggregate size or fractal dimension, since the effect of aggregate on absorption is completely neglected in RDG as stated in Equation (8). On the other hand, the absorption cross-sections from GMM vary somewhat significantly with both the aggregate size N_p and the fractal dimension D_f. It is noted that the nondimensional GMM absorption cross-sections are slightly higher than unity even for a single primary particle ($N_p = 1$). This is because GMM yields the Mie solution in this case, rather than the approximate Rayleigh solution. All three GMM curves in Figure 7 exhibit a similar trend: the normalized absorption cross-section first increases with the aggregate size and then decreases after it reaches a peak. Figure 7 also shows that the normalized aggregate absorption cross-section rises faster to reach a higher peak

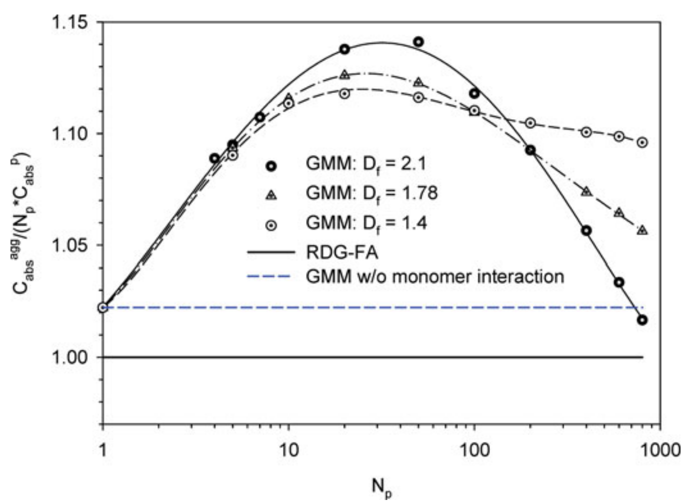

FIG. 7. Variation of nondimensional aggregate absorption cross-section with aggregate size for monodisperse aggregates of different fractal dimension. (Color figure available online.)

at a somewhat larger N_p and then decays faster after the peak as D_f increases. Under the conditions of this study RDG underestimates the aggregate absorption cross-section by about 12% to 14%, depending on D_f. As explained by Mulholland et al. (1994), there are two competing effects affecting the absorption of fractal aggregates: (i) for small aggregates the dipole–dipole coupling results in an increased exciting field, which, in turn, enhances the aggregate absorption, and (ii) for large aggregate the dipole–dipole coupling leads to a shielding effect, which reduces aggregate absorption. Therefore, the aggregate absorption cross-section peaks at a certain aggregate size as a result of these competing factors. The results shown in Figure 7 indicate that the dipole–dipole coupling effects (alternatively, interactions among primary particles, or multiple scattering effects) are stronger as D_f increases. It is also interesting that the effect of D_f on the normalized aggregate absorption cross-section shown in Figure 7 is weaker than the effect of primary particle size parameter ($\pi d_p/\lambda$) investigated in a previous study (Liu and Smallwood 2010b).

It should be pointed out that the absorption enhancement for small aggregates and the shielding effect for large aggregates are caused by the same mechanism—interactions among primary particles. To confirm that the variation of the aggregate cross-section with the aggregate size and the fractal dimension is indeed caused by the primary particle interaction, the results of aggregate cross-section for $D_f = 2.1$ without primary particle interactions were obtained and shown in Figure 7. The nondimensional GMM absorption cross-sections without primary particle interactions are independent of aggregate size and remain at the value of $N_p = 1$. This result confirms that the absorption enhancement for small aggregates and the shielding effect displayed for large aggregates are both attributed to the primary particle interactions.

The results of Liu et al. (2008) for $m = 1.75 + 0.5i$, $a = 15$ nm, and $\lambda = 870$ nm showed that the aggregate absorption cross-section for aggregates in the size range of 200 and 800 first decreases slightly with the fractal dimension when D_f is less than 2, but increases fairly quickly when the fractal dimension is greater than 2. In our results shown in Figure 7, the normalized aggregate absorption cross-section for aggregates of size between 200 and 800 decreases monotonically with increasing D_f for the relatively narrow range of 1.4 to 2.1 investigated. Based on the trend of variation of the absorption cross-section with aggregate size and fractal dimension shown in Figure 7 and the two competing factors affecting aggregate absorption (Mulholland et al. 1994), it is unlikely that the aggregate absorption cross-section will increase with increasing the fractal dimension beyond 2.1 for a fixed aggregate size between $N_p = 200$ and 800. Although the conditions of our study differ somewhat from those of Liu et al. (2008) in the refractive index of soot ($1.6 + 0.6i$ vs. $1.75 + 0.5i$), fractal prefactor (2.3 vs. 1.6), and wavelength (532 nm vs. 870 nm), none of these factors seems adequate to explain the potentially different trends in how aggregate absorption cross-section vary with D_f between our work and that of Liu et al. (2008). Further studies are required to confirm the trend obtained by Liu et al. (2008) by generating fractal aggregates of higher fractal dimensions but with a smaller fractal prefactor.

CONCLUSIONS

The effects of fractal dimension in the range of 1.4 and 2.1 on the radiative properties of numerically generated monodisperse fractal soot aggregates of a fixed prefactor of 2.3 at a wavelength of 532 nm were investigated using the RDG theory and GMM and an assumed soot refractive index of $1.6 + 0.6i$.

The structure factor affects the RDG scattering properties more significantly with increasing the fractal dimension. The structure factor of Köylü and Faeth is similar to that of Dobbins and Megaridis; however, a coefficient is missing in the power-law regime expression in the structure factor of Köylü and Faeth. As a result, the structure factor of Köylü and Faeth is not recommended. The structure factor of Sorensen is recommended to conduct RDG calculations. RDG predicts the scattering properties of fractal soot aggregates reasonably well even for fairly compact aggregates with a fractal dimension of 2.1. However, RDG fails completely to account for the effect of particle aggregation or the effect of morphological parameters of fractal soot aggregates on absorption, though the error caused by this failure is in general less than 15%.

The vertical–vertical differential scattering cross-section is sensitive to the fractal dimension. When plotted against the scattering angle, the vertical–vertical differential scattering cross-section decays slower with increasing the fractal dimension. However, when plotted against qR_g it decays faster with increasing the fractal dimension, which is simply due to the fact that for a given number of primary particles the aggregate radius of gyration decreases as D_f increases.

Results of RDG deviate from those of GMM in all the scattering properties examined. The magnitude of the discrepancy between RDG and GMM depends on the aggregate size and/or the fractal dimension. The difference between the RDG and GMM results is primarily attributed to the primary particle interactions, which are absent in the RDG theory. The primary particle interactions are responsible for the enhanced absorption and scattering for small aggregates and the weakened absorption and scattering for large aggregates. The total scattering cross-section of soot aggregates increases quite significantly with increasing the fractal dimension. At a higher fractal dimension, the effect of primary particle interactions on aggregate absorption cross-section becomes more important, leading to higher normalized absorption cross-section for small aggregates and lower normalized absorption cross-section for large aggregates. The effect of fractal dimension on soot aggregate radiative properties can be related to its effect on soot aggregate compactness. Because the fractal prefactor affects the fractal aggregate compactness in a similar way as D_f, i.e., a large k_f leads to a more compact structure, it is expected that k_f affects soot radiative properties in a qualitatively similar way as D_f, which is supported by the findings of Liu et al. (2009) on the effect of k_f on soot radiative properties.

Further studies are required to extend the range of the fractal dimension and to uncover the causes for the potential discrepancies between the present results and those published previously in the literature.

REFERENCES

Adachi, K., Chung, S. H., Friedrich, H., and Buseck, P. R. (2007). Fractal Parameters of Individual Soot Particles Determined Using Electron Tomography: Implications for Optical Properties. *J. Geophys. Res.* 112:D14202.

Berry, M. V., and Percival, I. C. (1986). Optics of Fractal Clusters Such as Smoke. *Optica Acta*, 33:577–591.

Bohren, C. F., and Huffman, D. R. (1983). *Absorption and Scattering of Light by Small Particles*. Wiley, New York.

Brasil, A. M., Farias, T. L., and Carvalho, M. G. (2000). Evaluation of the Fractal Properties of Cluster-Cluster Aggregates. *Aerosol Sci. Tech.*, 33:440–454.

Brown, D. M., Wilson, M. R., MacNee, W., Stone, V., and Donaldson, K. (2001). Size-Dependent Proinflammatory Effects of Ultrafine Polystyrene Particles: A Role for Surface Area and Oxidative Stress in the Enhanced Activity of Ultrafines. *Toxicol. Appl. Pharmacol.*, 175:191–199.

Cai, J., Lu, N., and Sorensen, C. M. (1995). Analysis of Fractal Cluster Morphology Parameters: Structural Coefficient and Density Autocorrelation Function Cutoff. *J. Colloid Interface Sci.*, 171:470–473.

Cross, E. S., Onasch T. B., Ahern, A., Wrobel W., Slowik, J. G., Olfert, J., et al. (2010). Soot Particle Studies—Instrument Inter-Comparison—Project Overview, *Aerosol Sci. Tech.*, 44:592–611.

Dobbins, R. A., and Megaridis, C. M. (1991). Absorption and Scattering of Light by Polydisperse Aggregates. *Appl. Optics*, 30:4747–4754.

Farias, T. L., Carvalho, M. G., Köylü, Ü. Ö., and Faeth, G. M. (1995). Computational Evaluation of Approximate Rayleigh-Debye-Gans/Fractal-Aggregate Theory for the Absorption and Scattering Properties of Soot. *ASME J. Heat Transfer*, 117:152–159.

Farias, T. L., Köylü, Ü. Ö., and Carvalho, M. G. (1996). Range of Ralidity of the Rayleigh-Debye-Gans Theory for Optics of Fractal Aggregates. *Appl. Opt.*, 35:6560–6567.

Filippov, A. V., Zurita, M., and Rosner, D. E. (2000). Fractal-Like Aggregates: Relation Between Morphology and Physical Properties. *J. Colloid Interface Sci.*, 229:261–273.

Forrest, S. R., and Witten Jr., T. A. (1979). Long-Range Correlations in Smoke-Particle Aggregates. *J. Phys. A: Math. Gen.*, 12:L109–L117.

Gmachowski, L. (2002). Calculation of the Fractal Dimension of Aggregates. *Colloids Surf. A*, 211:197–203.

Hasmy, A., Foret, M., Pelous, J., and Jullien, R. (1993). Small-Angle Neutron-Scattering Investigation of Short-Range Correlations in Fractal Aerosols: Simulations and Experiments. *Phys. Rev. B*, 48:9345–9353.

Heinson, W. R., Sorensen, C. M., and Chakrabarti, A. (2012). A Three Parameter Description of the Structure of Diffusion Limited Cluster Fractal Aggregates. *J. Colloid Interface Sci.*, 375:65–69.

Jacobson, M. Z. (2001). Strong Radiative Heating Due to the Mixing State of Black Carbon in Atmospheric Aerosols. *Nature*, 409:695–697.

Johnson, D. W., Kilsby, C. G., McKenna, D. S., Saunders, R. W., Jenkins, G. J., Smith, F. B., et al. (1991). Airborne Observations of the Physical and Chemical Characteristics of the Kuwait Oil Smoke Plume. *Nature*, 353:617–621.

Jullien, R., and Botet, R. (1987). *Aggregation and Fractal Aggregates*. World Scientific, Singapore.

Kazakov, A., and Frenklach, M. (1998). Dynamic Modeling of Soot Particle Coagulation and Aggregation: Implementation with the Method of Moments and Application to High-Pressure Laminar Premixed Flames. *Combust. Flame*, 114:484–501.

Kerker, M. (1969). *The Scattering of Light*. Academic Press, New York, pp. 414–486.

Khlebtsov, N. G. (1992). Orientational Averaging of Light-Scattering Observables in the T-Matrix Approach. *Appl. Opt.*, 31:5359–5365.

Köylü, Ü. Ö., and Faeth, G. M. (1993). Radiative Properties of Flame-Generated Soot. *ASME J. Heat Transfer*, 115:409–417.

Köylü, Ü. Ö., and Faeth, G. M. (1994). Optical Properties of Overfire Soot in Buoyant Turbulent Diffusion Flames at Long Residence Time. *ASME J. Heat Transfer*, 116:152–159.

Köylü, Ü. Ö., Xing, Y., and Rosner, D. E. (1995). Fractal Morphology Analysis of Combustion-Generated Aggregates Using Angular Light Scattering and Electron Microscopic Images. *Langmuir*, 11:4848–4854.

Lack, D. A., and Cappa, C. D. (2010). Impact of Brown and Clear Carbon on Light Absorption Enhancement, Single Scatter Albedo and Absorption Wavelength Dependence of Black Carbon. *Atmo. Chem. Phys. Discussions*, 10:785–819.

Lapuerta, M., Ballesteros, R., and Martos, F. J. (2006). A Method to Determine the Fractal Dimension of Diesel Soot Agglomerates. *J. Colloid Interface Sci.*, 303:149–158.

Liu, L., Mishchenko, M. I., and Arnott, W. P. (2008). A Study of Radiative Properties of Fractal Soot Aggregates Using the Superposition *T*-Matrix Method. *JQSRT*, 109:2656–2663.

Liu, F., and Smallwood, G. J. (2010a) Radiative Properties of Numerically Generated Fractal Soot Aggregates: The Importance of Configuration Averaging. *ASME J. Heat Transfer*, 132:023308-1–023308-6.

Liu, F., and Smallwood, G. J. (2010b). Effect of Aggregation on the Absorption Cross Section of Fractal Soot Aggregates and Its Impact on LII Modelling. *JQSRT*, 111:302–308.

Liu, F., and Snelling, D. R. (2008). Evaluation of the Accuracy of the RDG Approximation for the Absorption and Scattering Properties of Fractal Aggregates of Flame-Generated Soot. 40th Thermophysics Conference, AIAA 2008–4362, Seattle, Washington.

Liu, F., Snelling, D. R., and Smallwood, G. J. (2009). Effects of the Fractal Prefactor on the Optical Properties of Fractal Soot Aggregates. MNHMT2009-18473, ASME 2009 2nd Micro/Nanoscale Heat & Mass Transfer International Conference, Shanghai, China.

Mikhailov, E. F., Vlasenko, S. S., Krämer, L., and Niessner, R. (2001). Interaction of Soot Aerosol Particles with Water Droplets: Influence of Surface Hydrophilicity. *J. Aerosol Sci.*, 32:697–711.

Mishchenko, M. I. (1991). Light Scattering by Randomly Oriented Axially Symmetric Particles. *J. Opt. Soc. Am. A*, 8:871–882.

Mishchenko, M. I., Videen, G., Khlebtsov, G., Wriedt, T., and Zakharova, N. T. (2008). Comprehensive T-Matrix Reference Database: A 2006–2007 Update. *JQSRT*, 109:1447–1460.

Mulholland, G. W., Bohren, C. F., and Fuller, K. A. (1994). Light Scattering by Agglomerates: Coupled Electric and Magnetic Dipole Method. *Langmuir*, 10:2533–2546.

Oberdörster, G., Sharp, Z., Atudorei, V., Elder, A., Gelein, R., Kreyling, W., and Cox, C. (2004). Translocation of Inhaled Ultrafine Particles to the Brain. *Inhalat. Toxicol.*, 16:437–445.

Oh, C. and Sorensen, C. M. (1997). The Effect of Overlap Between Monomers on the Determination of Fractal Cluster Morphology. *J. Colloid Interface Sci.*, 193:17–25.

Ouf, F. X., Yon, J., Ausset, P., Coppalle, A., and Maille, M. (2010). Influence of Sampling and Storage Protocol on Fractal Morphology of Soot Studied by Transmission Electron Microscopy. *Aerosol Sci. Tech.*, 44:1005–1017.

Reid, J. S., and Hobbs, P. V. (1998). Physical and Optical Properties of Young Smoke from Individual Biomass Fires in Brazil. *J. Geophys. Res.*, 103:32013–32030.

Singham, S. B., and Bohren, C. F. (1993). Scattering of Unpolarized and Polarized Light by Particle Aggregates of Different Size and Fractal Dimension. *Langmuir*, 9:1431–1435.

Sorensen, C. M. (2001). Light Scattering by Fractal Aggregates: A Review. *Aerosol Sci. Tech.*, 35:648–687.

Sorensen, C. M., Cai, J., and Lu, N. (1992). Test of Static Structure Factors for Describing Light Scattering from Fractal Soot Aggregates. *Langmuir*, 8:2064–2069.

Sorensen, C. M., and Feke, G. D. (1996). The Morphology of Macroscopic Soot. *Aerosol. Sci. Tech.*, 25:328–337.

Sorensen, C. M., and Roberts, G. C. (1997). The Prefactor of Fractal Aggregates. *J. Colloid Interface Sci.*, 186:447–452.

Van-Hulle, P., Weill, M.-E., Talbaut, M., and Coppalle, A. (2002). Comparison of Numerical Studies Characterizing Optical Properties of Soot Aggregates for Improved EXSCA Measurements. *Part. Part. Syst. Charact.*, 19: 47–57.

Xu, Y.-L. (1995). Electromagnetic Scattering by an Aggregate of Spheres. *Applied Optics*, 34: 4573–4588.

Xu, Y.-L. (1997). Electromagnetic Scattering by an Aggregate of Spheres: Far Field. *Applied Optics*, 36: 9496–9508.

Xu, Y.-L., and Khlebtsov, N. G. (2003). Orientation-Averaged Radiative Properties of an Arbitrary Configuration of Scatterers. *JQSRT*, 79–80: 1121–1137.

Yang, B., and Köylü, Ü. Ö. (2005). Soot Processes in a Strongly Radiating Turbulent Flame from Laser Scattering/Extinction Experiments. *JQSRT*, 93:289–299.

Yon, J., Roze, C., Girasole, T., Coppalle, A., and Mees, L. (2008). Extension of RDG-FA for Scattering Prediction of Aggregates of Soot Taking into Account Interactions of Large Monomers. *Part. Part. Syst. Char.*, 25: 54–67.

Zhang, R., Khalizov, A. F., Pagels, J., Zhang, D., Xue, H., and McMurry, P. H. (2008). Variability in Morphology, Hygroscopicity, and Optical Properties of Soot Aerosols During Atmospheric Processing. *PNAS*, 105:10291–10295.